EFDA–JET–CP(12)06/32

G. Arnoux, T. Farley, C. Silva, S. Devaux, M. Firdaouss, D. Frigione,
R. Goldston, J. Gunn, J. Horacek, S. Jachmich, P.J. Lomas, S. Marsen,
G.F. Matthews, R.A. Pitts, M. Stamp, P. Stangeby
and JET EFDA contributors

Scrape-Off Layer Properties of ITER-Like Limiter Start-up Plasmas at JET

Scrape-Off Layer Properties of ITER-Like Limiter Start-up Plasmas at JET

G. Arnoux[1], T. Farley[2], C. Silva[3], S. Devaux[4], M. Firdaouss[5], D. Frigione[6], R. Goldston[7], J. Gunn[5], J. Horacek[8], S. Jachmich[9], P.J. Lomas[1], S. Marsen[10], G.F. Matthews[1], R.A. Pitts[11], M. Stamp[1], P. Stangeby[12] and JET EFDA contributors*

JET-EFDA, Culham Science Centre, OX14 3DB, Abingdon, UK

[1]EURATOM-CCFE Fusion Association, Culham Science Centre, OX14 3DB, Abingdon, OXON, UK
[2]University of Bristol, Tyndall Avenue, Bristol, BS8 1TL, UK
[3]Associação EURATOM/IST, Instituto de Plasmas e Fusão Nuclear, Instituto Superior Técnico, Avenue Rovisco Pais, 1049-001 Lisbon, Portugal
[4]Max-Planck-Institut für Plasmaphysik, EURATOM-Assoziation, 85748 Garching, Germany
[5]Association EURATOM-CEA, CEA/DSM/IRFM, Cadarache 13108 Saint Paul Lez Durance, France
[6]Associazione EURATOM-ENEA sulla fusione, C.R Frascati, Roma, Italy
[7]Princeton Plasma Physics Laboratory, Princeton, NJ 08543, USA
[8]Association EURATOM-IPP.CR, Institute of Plasma Physics AS CR, Za Slovankou 3, 182 21 Praha 8, Czech Republic
[9]Association "EURATOM - Belgian State" Laboratory for Plasma Physics Koninklijke Militaire School - Ecole Royale Militaire Renaissancelaan 30 Avenue de la Renaissance B-1000 Brussels Belgium
[10]Max-Planck-Institut für Plasmaphysik, Teilinstitut Greifswald, EURATOM Assoziation, 17491 Greifswald, Gemany
[11]ITER Organization, Route de Vinon sur Verdon, 13115 Saint Paul Lez Durance, France
[12]University of Toronto, Institute for Aerospace Studies, Toronto, M3H 5T6, Canada
** See annex of F. Romanelli et al, "Overview of JET Results", (24th IAEA Fusion Energy Conference, San Diego, USA (2012)).*

Preprint of Paper to be submitted for publication in Proceedings of the 24th IAEA Fusion Energy Conference (FEC2012), San Diego, USA 8th October 2012 - 13th October 2012

ABSTRACT.
Recent experiments at JET combining reciprocating probe measurements (upstream) and infrared thermography (at the plasma facing components (PFC)) on plasmas in limiter configurations show that the common approach to predicting the power load on the limiter underestimates the heat flux at the contact point by a factor 1.5 – 3. The current model and scaling laws used for predicting the power load onto the first wall during limiter current ramp-up/down in ITER are uncertain and a better understanding of the heat transport to the PFCs is required. The heat loads on PFCs are usually predicted by projecting the parallel heat flux associated with scrape-off layer (SOL) properties at the outer mid-plane (upstream) along the magnetic field lines to the limiter surface and deducing the surface heat flux through a cosine law, thus ignoring any local effect of the PFC on transport within the SOL. The underestimate of the heat flux is systematic in inner wall limiter configurations, independent of the plasma parameters, whereas in outer limiter configuration this is not observed, probably because of the much shorter SOL power decay length. Models that can explain this enhanced heat flux around the contact point are proposed and discussed but at this stage one cannot give a final conclusion.

1. INTRODUCTION

The plasma power load onto the first wall plasma facing components (PFC) during the current ramp-up/down in ITER must be minimised in order to avoid possible melting of the beryllium tiles which armour the actively cooled first wall [1]. The commonly employed technique to predict power loads onto the PFCs, q_{lim}, is to start from an assumed scrape-off layer (SOL) heat flux profile, $q_{||}(r_{mid})$, at the outer mid-plane, omp, where r_{mid} is the radial distance from the omp the last closed flux surface (LCFS) and project these properties along the magnetic field lines, **B**, to the PFCs such that:

$$q_{lim} = (R_{LCFS}/ R_{lim}) \cdot \cos(\theta_n) \cdot q_{||} \quad (1)$$

with $\cos(\theta_n) = \hat{n} \cdot \mathbf{B}/||B||$ and $\hat{n}$ the normal vector to the PFC surface. The ratio R_{LCFS}/R_{lim} accounts for the flux expansion with R_{LCFS} the radial position of the LCFS at the omp and R_{lim} the radial position of the plasma contact point on the limiter. The heat flux profile is further assumed to be exponential such that:

$$q_{||}(r_{mid}) = q_{0||} \cdot e^{-r_{mid}/\lambda_q} \quad (2)$$

where $q_{0||}$ is the heat flux at the LCFS and λ_q the power decay length. This is the method employed, for example, by the field line tracing and surface heat flux calculation code PFCFLUX [2], which will be used below to compare with experimental infrared (IR) measurements.

Previous publications [3], [4] discussed the conditions when it is appropriate (and inappropriate) to project q||(rmid) along B, but the case of a limiter plasma was not examined there. It was observed

20 years ago that q_{lim} in the vicinity of the limiter tangency point is higher than the simple cosine law would predict [5]-[9]. The new measurements in JET limiter plasmas reported here show no exceptions in a large data set. As illustrated in the example of Figure 1(d) the gradient of the inferred $q_{||}$ is much steeper in the near SOL ($r_{mid} \leq 5$mm, $\lambda_{q,near} = 5.5$mm) than in the far SOL ($\lambda_q = 22$mm). This profile was derived from IR camera measurements of qlim on the limiter surface and projected back to the outer midplane using equation (1). Independent measurements in the SOL upstream of the limiter using a fast reciprocating Langmuir Probe (RCP), indicate that upstream profiles do follow an exponential decay (see Figure1 (b) and (c)), although the region of r_{mid} <5mm is could not be accessed by the probe in the experiments here. Furthermore, this effect is observed only in IWL configurations. The question is then: "is the enhanced heat flux observed in the near SOL due to a local action of the limiter which is not captured in the free SOL? It is essential to answer this question and understand the physics behind it if one wants to be able to make accurate predictions of the power loads to the first wall in ITER. The question of what impact this has on the power handling of the JET limiters is addressed in a companion paper [10].

The present scaling used for ITER is based on L-mode diverted plasmas [11] and uses only RCP data. There is no credit given to any enhanced heat flux effect on the limiter surface which has been observed in the new JET data. Recent RCP measurements on Tore Supra (TS), over a large range of plasma current, I_p, plasma density, ne, and edge safety factor, q_{edge}, have shown that the present ITER scaling is unsatisfactory [12]. A new multi-machine scaling must be found for limiter configurations and is in the process of being compiled and analysed under the auspices of the International Tokamak Physics Activity (ITPA) Divertor and SOL physics Topical Group. In this contribution we discuss the JET database in the context of the inverse ohmic power law found with the TS data [12].

2. MEASUREMENTS AND METHOD

2.1. DETERMINATION OF THE INFERRED $q_{||}(r_{mid})$ WITH RCP MEASUREMENTS

The Langmuir probe measures the ion saturation current, I_{sat} and the electron temperature, T_e, derived from the current-voltage characteristic of the probe (Figure 1b and c). For sheathlimited conditions at the probe, and if $T_e = T_i$, $q_{||}(r_{mid}) = \gamma_{||} \Gamma_{||} (r_{mid}) T_e, (r_{mid})$ where $\gamma_{||}$ is the parallel sheath transmission factor and $\Gamma_{||} = I_{sat}/e$ with e the electron charge. The power decay length can be either deduced from the temperature decay length, λ_{Te} and the ion saturation current decay length, λ_{Isat} such that: $1/\lambda_q = 1/\lambda_{Isat} + 1/\lambda_{Te}$ or by fitting equation (2) to $q_{||}(r_{mid})$. The first method requires no knowledge of the absolute value of the heat flux. In the second case, $q_{||}(r_{mid})$ is usually estimated assuming a fixed value of $\gamma_{||}$ ($\gamma_{||}$= 8 here). More details of the RCP data can be found in [13]. The JET probe head is equipped with different pins and the resulting I_{sat} and T_e can depend on the analysis method and on which pin is used.

In this contribution, two sets of independently analysed data will be used (labelled RCP I and RCP II), leading to slightly different results.

2.2. DETERMINATION OF THE INFERRED $q_{||}(r_{mid})$ WITH IR MEASUREMENTS

The wide angle view IR system at JET [14] can measure the surface temperature, $T_{lim}(x, y, t)$, of the IWGL module 8Z and of the WOPL module 1D, both made of highly shaped, castellated, beryllium tiles [10], [15]. The heat load associated with each pixel (x, y), $q_{lim}(x, y,t)$, is derived from $T_{lim}(x, y, t)$ using the non-linear finite difference code THEODOR [16]. In the specific case of the JET limiters, because of the tile castellation (12×12mm) lateral diffusion (parallel to the PFC surface) can be neglected and the heat diffusion equation is resolved only into the depth of the tile. Note that the pixel resolution (~15–20mm) is of the same order as that of the castellation size. In our analysis $q_{lim}(x, y,t)$ is time averaged over a window of 500ms: $\langle q_{lim}(x, y,t)\rangle_t = q_{lim}(x, y,t)$.

To relate the inferred qlim (x, y) to the topology of a given magnetic equilibrium, the IR image of the limiter (Figure 2(a)) is mapped in 3D geometry to obtain a 2D surface in cylindrical coordinates: {R(x, y);z(x, y); ϕ(x, y)}, with R the radial position, z the vertical position and ϕ the toroidal position of the surface of the object seen by each pixel. A heat flux map can then be constructed, for example in the ϕ-z plane as illustrated in Figure 2(b). For a given magnetic equilibrium, the heat flux map qlim (ϕ,z) can be directly associated with an omp map, $r_{mid}(\phi,z)$ (Figure 2(c)) and a field line angle map, $\theta_n(\phi,z)$ (Figure 2(d)). Using the three maps: $q_{lim}(\phi,z)$, $r_{mid}(\phi,z)$ and $\theta_n(\phi,z)$ with equation (1) and (2) yields the inferred $q_{||}(r_{mid})$ profile as illustrated in the examples of Figure 1 (d) and (e). From a least-square fit, λ_q can then be derived. Only a selection of pixels in $q_{lim}(\phi,z)$ are used in this process (mask in Figure 2(e)). For the analysis here, we used three selection criteria: 1) The pixel must be in a wetted area (it must be connected to the omp). The flux map predicted by PFCFLUX in Figure 2(f) also shows the shadowed area (in grey) 2) The pixel must have $q_{lim} > 0$, in other words, it must have a significant heat load and not be affected by re-deposited layers, which are known to have poor thermal contact with the bulk of the tile. 3) For the IWGL, the pixel must be located on the electron drift side (left hand side) of the limiter. This latter criteria was imposed as a consequence of some ambiguities in the interpretation of the IR image on the ion drift side - the high heat flux area slightly above the contact point on the right hand side is not completely understood, even if a higher heat flux than on the electron drift side is expected due to asymmetry in the shadowing by neighbouring limiters.

Figure 1 shows the inferred $q_{||}(r_{mid})$ from the IR measurement for an IWL (d) and an OWL (e) configuration (see Figure 1(a) on loglinear scale and for comparable plasma parameters: P_{SOL} = 3.5MW, $n_{e,l} = 6.9\times10^{19}\,m^{-2}$, $I_p = 2.0$MA and $B_\phi = 2.7$T ($q_{edge} = 3.5$), where B_ϕ is the toroidal magnetic field, P_{SOL} the power crossing the LCFS and ne,l the line integrated density. Two main conclusions can be drawn from these examples, which are representative of the whole database: 1) The inferred parallel heat flux profile on the IWL is not a single exponential and has a much steeper gradient in the near SOL ($r_{mid} < 5$mm). The profile can be characterised by two exponential functions with different decay lengths: $\lambda_{q,far} = 20$mm and $\lambda_{q,near} = 5.5$mm for the far and near SOL respectively. 2) The parallel heat flux profile in the OWL is exponential and the power decay length is much smaller ($\lambda_q \cong 8$mm) than that of the IWL far SOL.

2.3. EXPERIMENTS

In order to contribute to a multi-machine scaling forlq , a dedicated scenario, optimised for the edge diagnostics, was repeated (for a total of 35 JET pulses) scanning the key operational parameters: the plasma current, $1.2 < I_p < 2.5$MA, the plasmas density (line integrated), $3.8 < n_{e,l,} < 8.0\times10^{19}$ m^{-2}, and the heating power, $0.7 < P_{heat} < 4.4$MW. The magnetic field was fixed, $B_\phi = 2.7$T, yielding a scan in q_{edge} through the I_p variation ($2.7 < q_{edge} < 6.9$). The different operational constraints on the two diagnostics (IR and RCP) did not allow complete coverage of the same parameter range. Whilst the IR measurements cover more values of I_p, $n_{e,l}$ and P_{heat}, the RCP data allow a wider range of comparison between IWL and OWL configurations.

2.4. VALIDATION OF THE MEASUREMENTS WITH A POWER BALANCE

The power entering the SOL can be derived from the following formula [17]:

$$P_{SOL} = 2\pi R_{LCFS} \frac{B_\theta}{B_\phi} \cdot \int_0^{r_{wall}} 2q_{\parallel}(r_{mid})dr_{mid} = 4\pi \frac{B_\theta}{B_\phi} \lambda_q q_{0\parallel} \quad (3)$$

where B_θ the poloidal components of the total magnetic field and the B-field components are evaluated at RLCFS. The second equality comes from using equation (2) and taking = ¥ wall r , but this is not applied to the IR IWL data because the profiles are not single exponential. Instead, the integral is evaluated using the two exponential functions. The power to the SOL can also be deduced from power balance:

$$P_{SOL} = P_{heat} - P_{rad} - dW_{th}/dt \quad (4)$$

where P_{rad} is the power radiated into the core plasma (measured with bolometers) and dWth/dt is the change in the energy confinement. Figure 3 shows PSOL,meas deduced from equation (3) as a function of PSOL,bal deduced from equation (4) for the IR and RCP measurements. The RCP measurements give a reasonable power balance within 70 and 110% for most of the data points (and two extreme data points at 138% and 53%). There is a string difference between IR data for IWL and OWL plasmas. The latter provide good power balance (~90%), but for the IWL, whilst agreement is reasonable at low PSOL (ohmic plasmas with Ip < 1.7MA) only ~50% power balance is achieved at higher PSOL. As explained earlier, the inferred q||(rmid) profiles for the IWL are based on measurements on the electron drift side only (see Figure 2 (e)), with the assumption that this is representative of the total heat load on all 10 IWGL, on both ion and electron drift sides. The map of qlim in Figure 2(b), however, suggests that the heat load is in fact higher on the ion-drift side. Indeed, to fulfil the power balance the power load on the ion drift side should be ~3x higher than the electron drift side. There is also evidence that the heat loads are not evenly shared between the 10 IWGL [10] and this may explain why the power balance is not closed. The matter is the subject on on-going investigations. Note that the ratio PSOL,IR/PSOL,bal is strongly correlated with Ip,

which suggests that the heat load asymmetry increases with higher field line angles (lower q_{edge}). This asymmetry is not observed for the OWL configuration and we use both sides of the limiter to derive $q_{\|}(r_{mid})$.

3. DISCUSSION

3.1. IWL AND OWL CONFIGURATIONS

JET results systematically show a strong asymmetry in λ_q between IWL and OWL configurations: $\lambda^{IWL}_{q,\,RCP}$/ $\lambda^{OWL}_{q,\,RCP}$ and $\lambda^{IWL}_{q,\,I}$ / $\lambda^{OWL}_{q,\,IR}$. It has already been observed on several tokamaks that the plasma outflux is localised in a region around the omp. Experiments on TS, for example, indicate that the enhanced low field side outflux occurred over a poloidal extent of $\sim\theta = \pm 30^{o}$ around the omp [18]. In the JET experiments described here, the connection length (between the limiter and omp) is much shorter for OWL ($L_c^{OWL} \cong 1.2$m in JET) than for IWL ($25 < L_c^{IWL} < 52$m in the JET limiter plasmas studied here) and can explain this asymmetry in lq but it is not clear whether this is the dominant effect. Recycling and impurity (beryllium in JET) influx also appear to be different, especially in neutral beam heated (NBI) plasmas. A maximum of $Z_{eff} = 2.6$ is found for IWL cases at the highest NBI power whereas Z_{eff} reaches 3.8 in a similar case in OWL plasmas. The level of SOL turbulence is also found to be much smaller for OWL [13], which is consistent with a shorter λ_q. The factor 2 difference found between the IR and RCP measured ratio (IWL/OWL) is mainly due to the fact that $\lambda^{IWL}_{q,\,far\,,IR} \cong (0.6 \pm 0.1)\, \lambda^{IWL}_{q,\,RCP}$ for $I_p > 1.7$MA and that $\lambda_c^{OWL} \cong 8 \pm 1$ mm for all the measurements, independently of the diagnostic and plasma parameters. Note that for the IR, a direct comparison was only possible for two pulses at high beam power (the two highest P_{SOL} in Figure 3).

Recent work on TS has shown that the power decay length in IWL configuration depends on the ohmic power: a $\lambda_q = C \times P$ ohmic where C and a are fit coefficients [12]. Two different scaling laws have in fact been found on TS depending on the type of probe and method used. Figure 4 compiles λ_q for the JET IWL plasmas (IR and RCP) and TS (RCP) databases as a function of the heating power normalised to the plasma volume: P_{heat}/V_{plasma}. Note that for JET IR data, only $\lambda_{q,\,far}$ has been used in this plot. The two scaling laws found in [12] are also indicated. The IR points are in line with the scaling law derived from the RFA+TUN method (TS data not shown here) when $P_{heat}/V_{plasma} > 15$.

3.2. ENHANCED DEPOSITED HEAT FLUX NEAR THE LIMITER TANGENCY POINT

The inferred parallel heat flux profiles in IWL configurations, reconstructed from the IR measurements using the cos(qn) law systematically show an enhanced heat flux (see examples in Figure 1d and Figure 5) in the near SOL ($r_{mid} < 5$mm). This results from the higher heat flux measured around the contact point (centre of Figure 2(b)) than would be predicted with PFCFLUX (Figure 2(f)). The same effect has been observed in one example case on TS [19], but this was not systematically explored at the time. These profiles are characterised by a double exponential with separate decay lengths: $\lambda_{q,near}$ and $\lambda_{q,far}$. On average, $\lambda_{q,near}$ and $\lambda_{q,far} = 0.22 \pm 0.10$. The inferred heat flux at the LCFS, $q_{0,\|}$,

is 1.5 – 3 times higher than that predicted using a simple extrapolation from the far SOL profile. The consequence on the limiter is that the heat load around the contact point is 1.5–3 times higher than what the cos (θ_n) law would predict. The latter instead predicts $q_{lim,max}$ on the wings of the limiter (Figure 2(f)) whereas the measurements (Figure 2(b)) show qlim,max at the contact point [10].

The most likely explanation of the enhanced heat flux is the local sink action of the limiter, the socalled "funnel" effect [5]-[9]. The $q_{||}$ profiles (Figure 5) systematically show a scatter around the fit value of ±1 MW/m^2, with a clear systematic dependence on cos (θ_n). If the cos (θ_n) law held true, one would expect this scatter distribution to be independent of cos (θ_n). Let us define the residual $\delta q_{||} = (r_{mid}, \theta_n) - \bar{q}_{||}(r_{mid})$ where $\bar{q}_{||}(r_{mid})$ is the fit function described by two exponentials (with a discontinuity at r_{mid} = 6mm) and $q_{||}(r_{mid}, \theta_n)$ represents the data points. Figure 6 shows $\delta q_{||}$ as a function of θ_n for the example of the profile in Figure 5. The near and far SOL data are distinguished by different symbols. This clearly shows that $\delta q_{||}$ is strongly correlated with θ_n in the near SOL, which can also be seen as a measure of the toroidal distance from the limiter crown. In other words the limiter geometry plays a significant role in the near SOL. This is a strong indication that it is not upstream SOL physics but rather the local sink action of the limiter which is responsible for this enhanced heat flux. The fact that this "funnel" effect has not been observed in a divertor configuration [20] suggests that it is not only the grazing angle which is important but also the distance of the LCFS from the limiter surface.

Recently it has been shown numerically that solutions of the 2D non-linear heat diffusion equation exhibit strongly enhanced heat fluxes at the surface of a protruding object in the SOL of divertor plasmas [4]. This can be understood by noting that a sharp cold object attracts diffusive heat flux, similar to the enhanced local electrostatic field generated on the vicinity of a grounded electrical (both are governed by the Poisson equation). This analysis has been generalized to a 2D limiter geometry constructed to be analogous to the 3D JET inner limiter geometry. The finding is that the heat flux is again concentrated by the limiter, with a $(1/r_{mid})^{1/2}$ divergence in the effective $q_{||}$. The total heat flux reaches twice the extrapolated background heat flux at $r_{mid} \sim \lambda_{q,\,far}/8$ for a range of simulated λ_q, far similarly to what is observed experimentally, and thus corresponds to a small fraction of the total heat flux. It arises because the JET inner limiters have a sharp edge at their centre (along the poloidal direction), which determines the contact point. The numerical calculations indicate that this enhanced heat flux could be eliminated by use of parabolically shaped limiter crown, which provides a cancelling divergence in ds/dr_{mid}, where s represents distance along the divertor surface. It should be noted that the numerical calculations assume a conduction-limited regime ignoring spatial density variation and assuming Spitzer-like parallel heat diffusivity: $\chi_{||} \propto T_e^{5/2}$ and Bohm-like $\chi_{\perp} \propto T_e$. It is not clear that JET plasmas are fully in such a regime. Further studies are necessary to quantify this effect and see if it can be combined with the "funnel" effect described in reference [5]-[9].

CONCLUSION

The important issue of first wall panel power loads to be expected on ITER during limiter start-up/ramp down has been addressed in dedicated experiments on JET in which SOL power profiles have been measured both by Langmuir probes in the main SOL and IR thermography of limiter tile surfaces. For high field side (inner wall) limiter configurations, which ITER expects to use widely for start-up, the IR data unequivocally show a region of high heat flux in the vicinity of the tangency point, where the JET tile design is such that there is reasonably sharp ridge in the centre of the tile, but at which conventional field line mapping assuming the usual exponential profile of parallel power flow in the main SOL finds low surface power densities. The JET reciprocating probe does indeed find such a profile, whose characteristic width is consistent with IR data mapped back along SOL field lines for radial distances a few mm outside the LCFS. This anomalous tangency point heat flux seen at the inner wall is not, however, found on low field side limiter tiles in outer limiter configurations, even though the tile design is similar to those on the inner wall. The enhanced inner wall feature may be a consequence of a particle funnelling effect reported in the past from other devices, or possibly as a result of diffusive "attraction" of the heat flux at the limiter ridge. Numerical calculations of this latter effect in simplified geometry yield results not inconsistent with the experimental observation. These experiments demonstrate that conventional field line mapping of exponential SOL power profiles onto ITER inner wall limiter surfaces may not provide the correct surface power load distribution, but understanding of the physics driving the enhanced heat load is as yet insufficient to extrapolate the effect to ITER.

ACKNOWLEDGEMENT

This work, supported by the European Communities under the contract of Association between EURATOM and CCFE, was carried out within the framework of the European Fusion Development Agreement. The views and opinions expressed herein do not necessarily reflect those of the European Commission. This work was also part-funded by the RCUK Energy Programme under grant EP/I501045.

REFERENCES

[1]. Pitts, R.A., et al., Journal of Nuclear Materials, **415** (2011) S957-S964
[2]. Firdaouss, M., et al., Proceeding of 20th PSI conference (2012) Aachen, Germany
[3]. Goldston, R., Physics of Plasma, **17** (2010) 012503
[4]. Goldston, R., Journal of Nuclear Materials, **415** (2011) S566-S569
[5]. Matthews, G.F., et al., Plasma Physics and Controlled Fusion, **32** (1990) 1301
[6]. Stangeby, P, et al., Nuclear Fusion, **32** (1992) 2079
[7]. Guilhem, D., J. Hogan, T. Aniel, et al, Journal of Nuclear Materials **266-269** (1999) 272
[8]. Skinner, C.H., Journal of Nuclear Materials, **266-269** (1999) 940-946
[9]. Gray, D.S., M. Baelmans, J.A. Boedo, et al, Physics of Plasmas, **6** (1999) 2816

[10]. Nunes, I., et al., This conference (2012)
[11]. ITER Physics Expert Group on Divertor, Nuclear Fusion, **39** (1999) 2391
[12]. Gunn, J., et al, Proceeding of 20th PSI conference (2011) Aachen, Germany
[13]. Silva, C., et al., Proceeding of 20th PSI conference (2012) Aachen, Germany
[14]. Gauthier, E., et al., Fusion Engineering and Design, **82** (2007) 1335-1340
[15]. Riccardo, V., et al., Proceeding of 27th SOFT conference (2012) Liege, Belgium
[16]. Herrmann, A., et al., Plasma Physics and Controlled Fusion **37** (1995) 17-29
[17]. Rudakov, D., Journal of Nuclear Materials, **415** (2011) S387
[18]. Gunn, J., et al, Journal of Nuclear Materials, **363-365** (2007) 484-490
[19]. Carpentier, S., et al., Journal of Nuclear Materials, **390-391** (2009) 955-958
[20]. Matthews, G.F., et al., Nuclear Fusion, **31** (1991) 1383

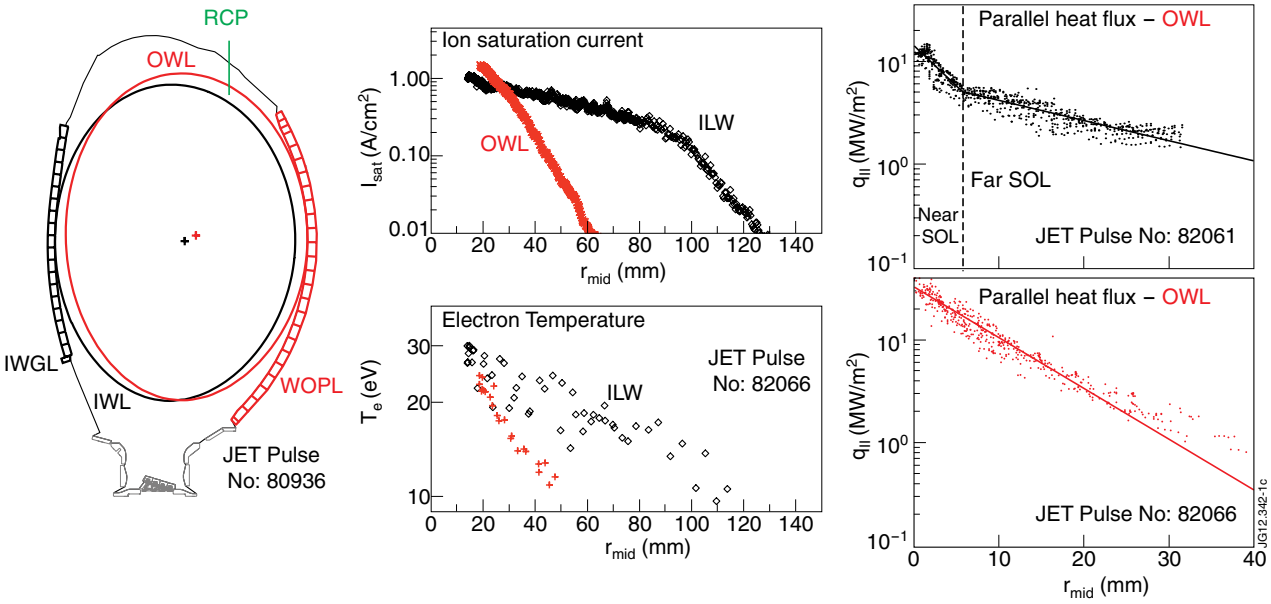

Figure 1: (a) JET cross-section with LCFS of two typical magnetic configurations, one limited on the inner wall guard limiters (IWGL) the other on the wide outer poloidal limiters (WOPL). (b) and (c) RCP measured ion saturation current and electron temperature profiles respectively, for an outer (OWL) and inner (IWL) limiter configuration. Note that the measurement are taken for $10 < r_{mid} < 130$mm. (d) and (e) inferred parallel heat flux profiles mapped to the omp, determined from the IR measurement at the limiter, of an IWL and OWL configuration respectively. Note that the IR measurements correspond only to the interval $0 < r_{mid} < 40$mm.

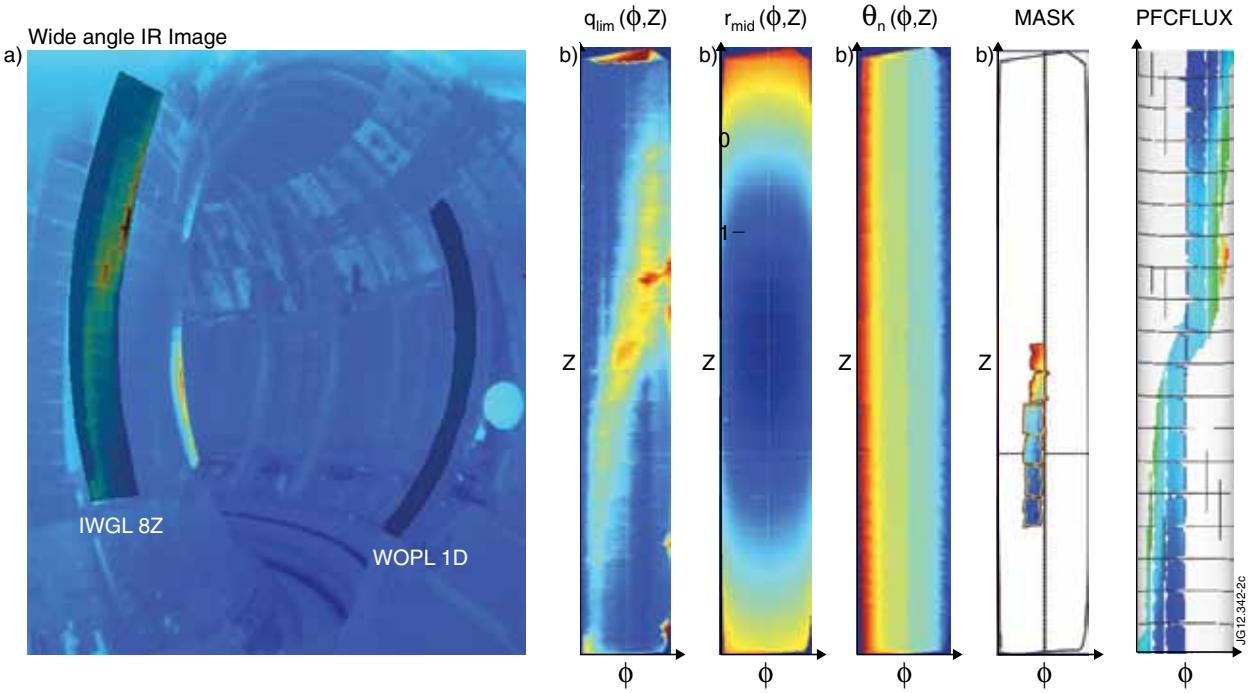

Figure 2: (a) Image taken by the IR wide angle view camera (KL7) in JET, Pulse No: 80836. Dark red indicates the brightest (hottest) areas. Shaded areas delimit the key PFCs analysed in this paper. (b) map in the (z,ϕ) co-ordinate of the IR measured heat flux on the IWGL 8Z, (c) the corresponding omp radius, r_{mid}, (d) the field line angle with respect to the normal vector to the PFC surface, θ_n, (e) mask (coloured region) of the pixels selected for the analysis, (f) the heat flux predicted by PFCFLUX (using λ_q = 30mm and P_{SOL} = 1.6MW).

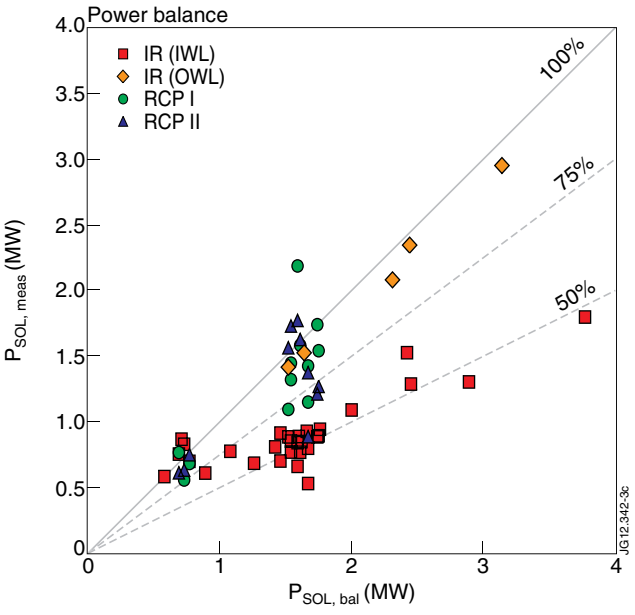

Figure 3: P_{SOL} determined from IR and RCP profile measurements (equation (3)) as a function of P_{SOL} derived from power balance (equation (4)).

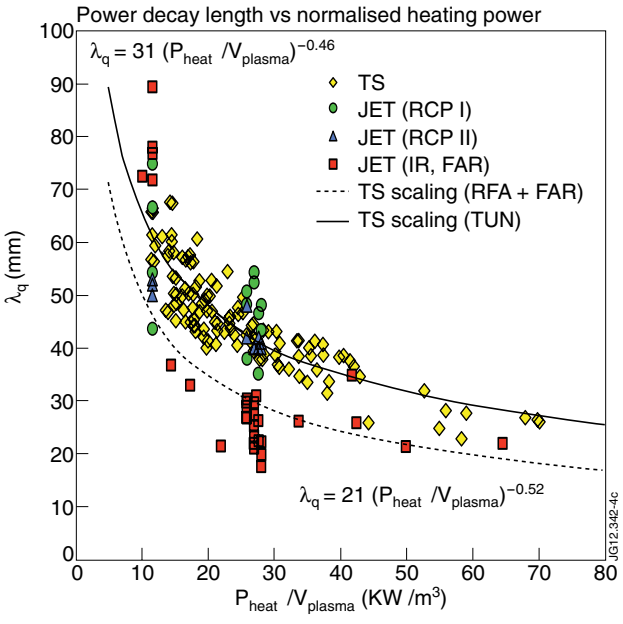

Figure 4: JET far SOLL power decay length, measured with RCP (circles and triangles) and with IR (squares) compared with RCP measurements (diamonds) on TS, as a function of the heating power normalised to the plasma volume. The two scaling laws based on TS data are also shown.

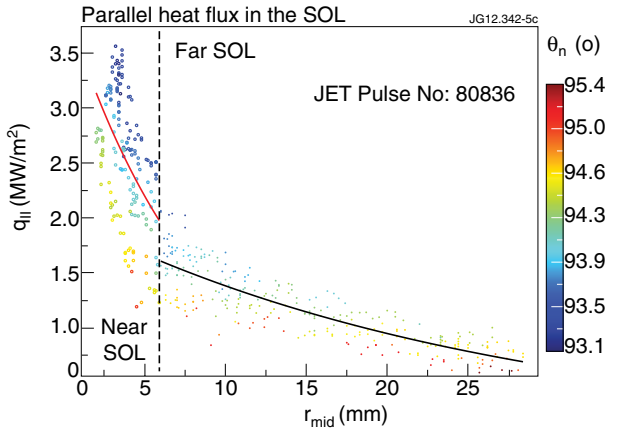

Figure 5: Inferred parallel heat flux profile derived from the IR measurement on the IWGL 8Z as a function of rmid. The colour bar indicates the field line angles on the limiter surface. Note that $93^o < \theta_n < 95^o$, which means that the field lines are never perfectly tangential to the limiter ($\theta_n = 90^o$). The data are fitted with two exponentials, one for each of the near and far SOL.

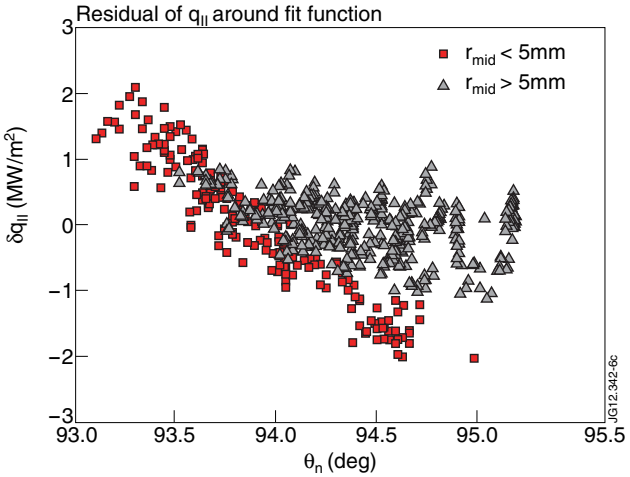

Figure 6: Residuals from the fit function as a function of the field line angle on the limiter surface, JET Pulse No: 80836.